HYDROTHERMAL SYNTHESIS AND ENHANCED PHOTOCATALYTIC ACTIVITY OF TiO$_2$-Fe@CNTs NANOCOMPOSITE FOR METHYLENE BLUE DEGRADATION UNDER VISIBLE LIGHT IRRADIATION

LE HA CHI, PHAM DUY LONG, NGUYEN VAN CHUC, AND LE VAN HONG
Institute of Materials Science, Vietnam Academy of Science and Technology

E-mail: chilh@ims.vast.ac.vn

Abstract. *TiO$_2$ is one of the most attractive metal oxides because of the excellent chemical and photocatalytic properties. However, a problem in the application of TiO$_2$ is the large band gap energy of 3.2 eV, corresponding to its photocatalytic activity under UV-light irradiation of wavelengths < 387 nm. In this work, TiO$_2$ nanoparticles doped with iron were grown on the surface of functionalized carbon nanotubes (TiO$_2$-Fe@CNTs) to expand the photoabsorbance of the nanocomposite materials in the visible light region and improve their photocatalytic activity. TiO$_2$-Fe@CNTs nanocomposite materials were synthesized by hydrothermal route in Teflon-sealed autoclave at 180°C for 10h. The FE-SEM and X-Ray diffraction measurements were taken for morphology and structural analysis of TiO$_2$ nanoparticles doped with Fe coating on CNTs. The effects of the iron and CNTs on the enhanced photocatalytic activity for methylene blue degradation under AM 1.5 illumination of 100 mW.cm^{-2} were investigated.*

Keywords: TiO$_2$, photocatalysis, nanotechnology.

I. INTRODUCTION

Titanium dioxide (TiO$_2$) has been extensively used semiconductor in solar cells, gas sensors, photocatalysis and photochemical processes due to its stability, low cost and non-toxicity [1]. However, narrow light response range under UV-light irradiation of wavelengths < 387 nm (corresponding to TiO$_2$ band gap energy about 3.2 eV) which accounts only for 4% of the incoming solar energy and low separation probability of the photoinduced electron – hole pairs in TiO$_2$ limits its technological applications. Therefore, doping of TiO$_2$ semiconductor nano-particles with transition metal ions including Fe, Cu, Ni or nonmetal atoms such as N, S, C to shift the optical absorption of from UV to the visible light region has been increasingly studied [2,3]. Doping TiO$_2$ with other elements can lead to a lower band gap and therefore improve the sunlight utilization of TiO$_2$. Additionally, the recombination of electron–hole pairs is suppressed by the introduction of other elements. Recently, the effect of co-doping TiO$_2$ with both cation and anion on the photocatalytic activity, such as Fe and Eu [4], Zn and Fe [5], N and Ni [6], N and S [7], shows apparently higher photocatalytic activity than that of a single doped TiO$_2$. Among the metals doped TiO$_2$, Fe doped TiO$_2$ show greatly improved photocatalytic activity compared to crude TiO$_2$. Fe is an

abundant element, environmentally friendly and suitably inserted into the TiO$_2$ lattice structures, because the ionic radius of iron (0.65 Å) and titanium (0.605 Å) is similar [8]. In this work, we demonstrated a simple hydrothermal method to prepare TiO$_2$ nanoparticles doped with iron coating on the surface of functionalized carbon nanotubes (TiO$_2$-Fe@CNTs) nanocomposite material. This approach was expected to improve the photoactivity of TiO$_2$ in the visible light range by increasing the surface area, creating defect structures to induce space-charge separation and enlarge the absorption region. The obtained materials are characterized by different methods such as: X-ray diffraction (XRD), Field emission scanning electron microscopy (FE-SEM), transmission electron microscopy (TEM), UV–vis spectroscopy. The effects of the Fe and CNTs components on the properties of the TiO$_2$ were discussed. The photocatalytic activity of the prepared TiO$_2$-Fe@CNTs composite photocatalysts was evaluated by the degradation of methylene blue under simulated solar light irradiation.

II. EXPERIMENTAL

II.1. Preparation of nanostructured TiO$_2$ doped with iron

Nanostructured TiO$_2$ doped with iron (TiO$_2$-Fe) powder were prepared by sol-gel method, using titanium tetra isopropoxide (Ti[OC$_3$H$_7$]$_4$), Fe(NO$_3$)$_3$.9H$_2$O (dopant), ethanol, HNO$_3$ and de-ionized water. All the chemicals are of highest purity and commercially available. They were used without further purification. Desired amount of Fe(NO$_3$)$_3$·9H$_2$O (the molar Fe/Ti ratio in the starting materials is 0.6 at.%) was dissolved in the mixture of 17 ml ethanol, 1.6 ml de-ionized water and 0.4 ml concentrated HNO$_3$. The mixed solution was then slowly dropped into the mixture of 34 ml ethanol and 6 ml titanium tetra isopropoxide, and the final solution was stirred for 30 minutes. The obtained sol was maintained at room temperature for 48 h. The resulting sol was evaporated at 100 °C for 24 hours to gradually form organic brown-colored gel. The yellow or pale white TiO$_2$-Fe powders were obtained by calcination at 400 °C for 3 hours. Finally, the materials were obtained by filtrating and washing with ethanol and de-ionized water for several times, and then dried at 80 °C for 12 hours.

II.2. Preparation of TiO$_2$-Fe@CNTs nanocomposite material

TiO$_2$-Fe@CNTs composites were prepared by a hydrothermal method as follow. Firstly, the CNTs need to be treated with strong acid mixture of 1:3 HNO$_3$/H$_2$SO$_4$ (by volume) under reflux for 12 hours to functionalize surface of CNTs. Due to the inert property of CNTs, this step is necessary to add carboxylic groups (COOH) on to the surface of the CNTs in order to enable them to take part in reactions with the nanoparticles. The resulting solution was filtered and washed thoroughly with water and decantation was used to remove any remaining acid, followed by drying in an oven at 200°C. The obtained powder was designated as acid-functionalized multiwalled carbon nanotubes (CNT–COOH). In the next step, 10 mg of functionalized CNTs was dissolved in a solution of 40ml de-ionized water and 20ml ethanol mixture using ultrasonic treatment for 2h. Then, 6ml titania precursor, namely titanium tetra isopropoxide (Ti[OC$_3$H$_7$]$_4$) solution was dissolved in the mixture of 34 ml ethanol, 0.4 ml concentrated HNO$_3$, 1.6 ml de-ionized water and 48.2 mg Fe(NO$_3$)$_3$.9H$_2$O. The mixed solution was then added to the functionalized CNTs solution and stirred for another 2 hours at 60°C to get a homogeneous suspension. The suspension was then placed in a 200 ml Teflon-sealed autoclave and maintained at 180°C for 10 hours. Finally, the
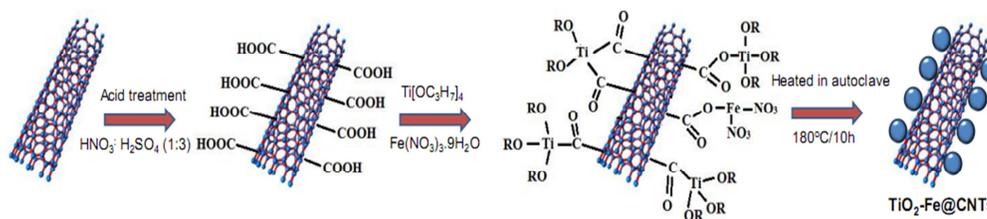
Fig. 1. Synthetic scheme for the preparation of TiO_2-Fe@CNTs nanocomposite material

resulting powder was recovered by filtration, rinsed by de-ionized water several times, and dried at 100°C for 12 hours.

II.3. Sample characterization

The surface morphology of samples was investigated by using a "Hitachi S-4800" field emission scanning electron microscopy (FE-SEM) and transmission electron microscopy (TEM, JEOL JEM1010). The crystalline phase was identified by X-ray diffraction (XRD) using a SIEMENS D5000 powder X-ray diffractometer (CuKα as radiation source, λ=0.15406 nm). The ultraviolet–visible (UV–vis) absorption spectra were performed by using a Jasco V-670 UV-VIS spectrometer.

II.4. Evaluation of photocatalytic performance

The photoreactor system used in the present work was measured under 1 sun illumination (100 mW.cm^{-2}, AM 1.5). For a typical experiment, 10 mg of catalyst was put into 20 ml of 0.01 g/l methylene blue (MB) aqueous solution with stirring in darkness for 30 min to reach the adsorption–desorption equilibrium of MB on the catalyst surface prior to illumination. The suspension was then exposed to light with continuous magnetic stirring. Then suspensions were collected and centrifugally separated every 20 min, and the filtrate was returned to the vial for measurement of the concentration MB degradation using a UV–vis spectrophotometer at a wavelength of 664 nm.

III. RESULTS AND DISCUSSION

III.1. Structure and morphology

Morphological characterization of TiO_2-Fe@CNTs nanocomposite material was carried out by FE-SEM (Fig. 2a) and TEM (Fig. 2b). As shown in Fig. 2a, FE-SEM image of TiO_2-Fe@CNTs nanocomposite material exhibits the presence of nanoparticles on the surface of carbon nanotubes. Some clusters of 100 nm nanoparticles were either randomly immobilized on the surface of CNTs or densely collected among CNTs bundles. TEM image in Fig. 2b reveals that granular TiO_2-Fe nanoparticles with 7 nm in diameter was intimately bound to the surface of CNTs.

Fig. 3 shows the XRD characterization of the TiO_2-Fe nanoparticles and TiO_2-Fe@CNTs nanocomposite material. The XRD pattern also shows that intensities of 0.6 at.% Fe doped TiO_2 (Fig. 3a) were slightly higher than TiO_2-Fe@CNTs (Fig. 3b). As seen from Fig. 3b, the strong diffraction peak for the TiO_2-Fe@CNTs at the angle (2θ) of 25.8^o can be assigned to the C (002) reflection of the hexagonal graphite structure. There are intensity peaks corresponding to anatase
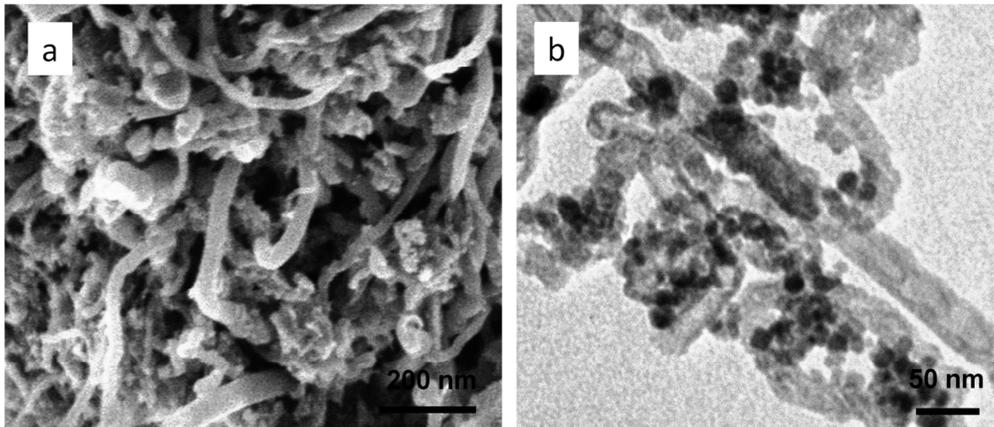
Fig. 2. FE-SEM (a) and TEM (b) images of the TiO$_2$-Fe@CNTs nanocomposite material

phase of TiO$_2$ for all samples without the appearance of trace rutile phase. No Fe peak was observed for either Fe doped TiO$_2$ or TiO$_2$-Fe@CNTs composite. This indicates that doping Fe ions with small percentages did not affect the crystalline structure of TiO$_2$ nanoparticles and no precipitate formation of doped metal such as iron oxides or Fe$_x$TiO$_y$. As noted previously [8,9], Fe^{3+} can be suitably inserted into the TiO$_2$ lattice structures and substituted Ti^{4+} site because the ionic radius of Fe^{3+} and Ti^{4+} is similar.
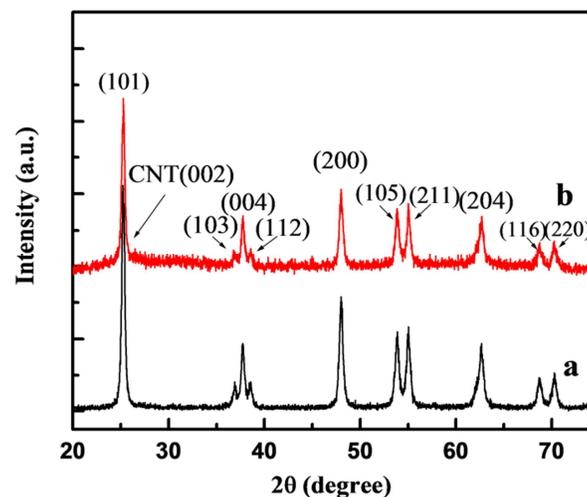

Fig. 3. XRD patterns of the TiO$_2$-Fe nanoparticles(a) and TiO$_2$-Fe@CNTs nanocomposite material (b).

III.2. Optical properties

To study the optical properties of Fe doped TiO_2 and TiO_2-Fe@CNTs samples, the UV–vis absorption spectra were measured, as shown in Fig. 4a. Compared with pure anatase TiO_2 that can only absorb $\lambda \leqslant 387$ nm UV light, the light absorption edges of Fe doped TiO_2 and TiO_2-Fe@CNTs nanocomposites move remarkably with a red shift to the visible range, as well as reduction in the bandgap energy.
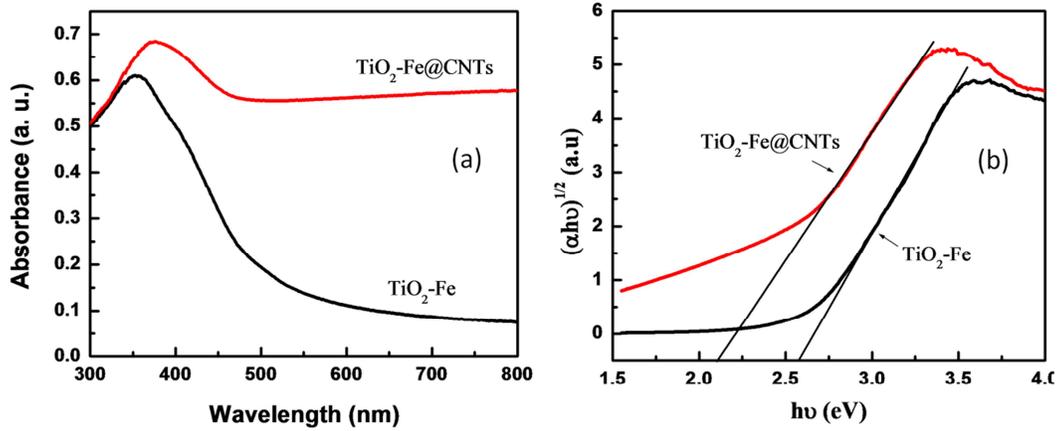

Fig. 4. UV–visible spectra (a) and plots of $(\alpha h\nu)^{1/2}$ as a function of photon energy (b) of the TiO_2-Fe nanoparticles and TiO_2-Fe@CNTs nanocomposite material.

The band gap energy Eg and absorption coefficient α are related by the following equation [10]:

$$\alpha h\nu = A(h\nu - E_g)^m$$

Where α is the absorption coefficient, $h\nu$ is the photon energy in eV, and E_g is the band gap energy in eV. A is a constant related to the effective mass of the electrons and holes and m being equal to 0.5 for allowed direct transition and 2 for an allowed indirect transition. Plots of between $(\alpha h\nu)^{1/2}$ and photon energy $(h\nu)$ for the TiO_2-Fe nanoparticles and TiO_2-Fe@CNTs nanocomposite material shown in the Fig. 4b. The energy gap Eg of the samples was evaluated from the intercept of the linear portion of the each curve with the $h\nu$ in X-axis. The straight lines imply that the TiO_2-Fe and TiO_2-Fe@CNTs nanocomposite samples have energy band gaps of 2.6 eV and 2.1 eV, respectively. The red shift in absorption spectrum and reduction in bandgap are attributed to the transfer of 3d-electrons from Fe to the conduction band of TiO_2.

III.3. Photocatalytic degradation of methylene blue

$\eta(\%) = \frac{C_o - C_t}{C_o} \times 100$ The photocatalytic degradation efficiency ($\eta\%$) could be calculated as the following equation:

where C_o is the initial absorbance of the MB solution and C_t, its absorbance at different irradiation times. All C values were obtained by the maximum absorption at 664 nm in the absorption spectrum in order to evaluate the degradation efficiency as shown in Fig. 5.
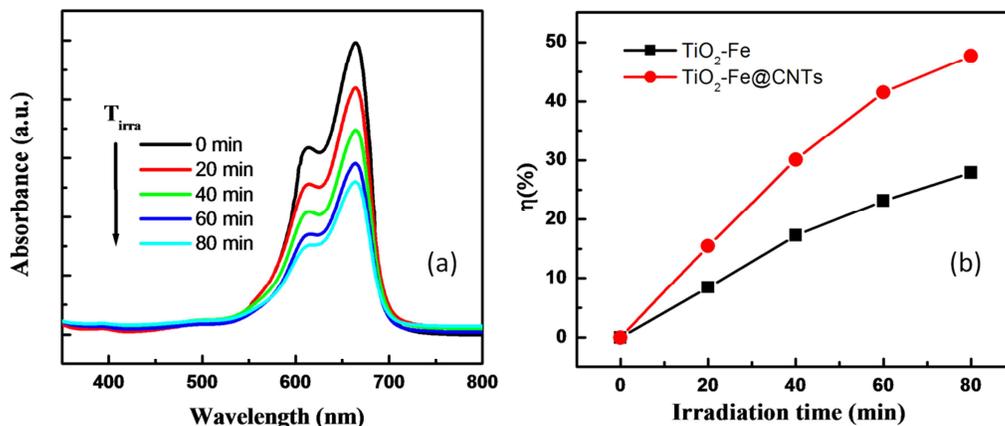
Fig. 5. Degradation indicated by absorption spectrum against TiO$_2$-Fe@CNTs photocatalyst (a) and the percentage degradation of methylene blue solutions under simulated solar light irradiation (b).
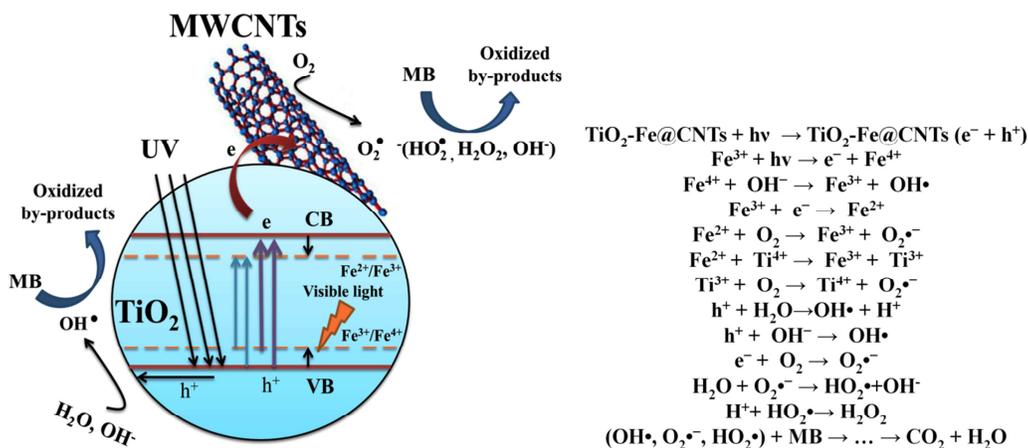

$$TiO_2\text{-}Fe@CNTs + h\nu \rightarrow TiO_2\text{-}Fe@CNTs \ (e^- + h^+)$$
$$Fe^{3+} + h\nu \rightarrow e^- + Fe^{4+}$$
$$Fe^{4+} + OH^- \rightarrow Fe^{3+} + OH\bullet$$
$$Fe^{3+} + e^- \rightarrow Fe^{2+}$$
$$Fe^{2+} + O_2 \rightarrow Fe^{3+} + O_2^{\bullet-}$$
$$Fe^{2+} + Ti^{4+} \rightarrow Fe^{3+} + Ti^{3+}$$
$$Ti^{3+} + O_2 \rightarrow Ti^{4+} + O_2^{\bullet-}$$
$$h^+ + H_2O \rightarrow OH\bullet + H^+$$
$$h^+ + OH^- \rightarrow OH\bullet$$
$$e^- + O_2 \rightarrow O_2^{\bullet-}$$
$$H_2O + O_2^{\bullet-} \rightarrow HO_2\bullet + OH^-$$
$$H^+ + HO_2\bullet \rightarrow H_2O_2$$
$$(OH\bullet, O_2^{\bullet-}, HO_2\bullet) + MB \rightarrow ... \rightarrow CO_2 + H_2O$$

Fig. 6. Schematic diagram of the separation of generated electrons and holes on the interface of TiO$_2$-Fe@CNTs photocatalyst under simulated solar light irradiation.

Enhanced activity of the TiO$_2$-Fe@CNTs photocatalyst in the visible light region as seen in the Fig. 5 is attributed to the formation of appearance of localized electronic gap states ascribed to Fe d–d or "localized charge transfer" transitions simultaneously. In addition, Ti–C and Ti–O–C defect sites in the TiO$_2$-Fe@CNTs photocatalyst act as trapping sites for photogenerated charges. When the catalyst is irradiated by photons, electrons (e$^-$) are excited from the valence band (VB) to the conduction band (CB) of Fe doped TiO$_2$ nanoparticles creating holes (h$^+$) in the VB. The hole (h$^+$) on the metal oxide nanoparticles oxidize hydroxyl groups to form hydroxyl radical (OH) which can decompose the methylene blue (MB). While CNTs act as a photo-generated electron

acceptor to promote interfacial electron transfer process and reduce the electron-hole recombination [11]. The adsorbed oxygen molecules on the surface of CNTs react with the electrons forming very reactive superoxide radical ion (O_2^-) which oxidize methylene blue (MB). The proposed photocatalytic methylene blue degradation mechanisms were described in the Fig. 6 and the reactions could be expressed as follows:

IV. CONCLUSIONS

TiO$_2$-Fe@CNTs nanocomposite photocatalyst was successfully prepared via hydrothermal synthesis. The structure, morphology and optical properties were investigated. The TiO$_2$-Fe@CNTs nanocomposite photocatalysts showed a high efficiency in the degradation of methylene blue under visible light. A tight interface between CNTs and TiO$_2$ doped with Fe was created. Doping TiO$_2$ with Fe ions can also expand its light absorption range to visible light through the formation of mid-gap states. On the other hand, CNTs with good adsorption capacity was successfully bonded with TiO$_2$ to reduce the electron-hole recombination rate and prevent the particles agglomeration. The higher visible light photocatalytic activity for methylene blue degradation of the TiO$_2$-Fe@CNTs nanocomposite was attributed to the increased adsorption capacity, enhanced light absorption and better charge separation. This semiconductor heterogeneous photocatalysis based on the advanced oxidation process (AOP) has enormous potential for the treatment of a wide range of organic contaminants in water.

ACKNOWLEDGMENT

REFERENCES

[1] T.L. Thompson and J.T. Yates, *Chem. Rev.* **106** (2006) 4428–4453.

[2] N. Serpone, *J. Phys. Chem. B* **110** (2006) 24287–24293.

[3] T.P. Ang, J.Y. Law and Y.F. Han, *Catalysis Letters* **139** (1-2) (2010) 77–84.

[4] L. Diamandescu, F. Vasiliu, D.T. Mihaila, M. Feder, A.M. Vlaicu, C.M. Teodorescu, D. Macovei, I. Enculescu, V. Parvulescu and E. Vasile, *Materials Chemistry and Physics* **112** (2008) 146–153.

[5] Z.H. Yuan, J.H. Jia and L.D. Zhang, *Materials Science Communications* **73** (2002) 323–326.

[6] J. Fan, E.Z. Liu, L. Tian, X.Y. Hu, Q. He and T. Sun, *J. Env. Eng. ASCE* **37** (2011) 171–176.

[7] F.Y. Wei, L.G. Ni and P. Cui, *Journal of Hazardous Materials* **156** (2008) 135–140.

[8] K. C. Christoforidis, A. Iglesias-Juez, S. J. A. Figueroa, M. Di Michiel, M. A. Newtonb and M. Fernandez-Garcı, *Catal. Sci. Technol.* **3** (2013) 626-634.

[9] S.Wang, J.S. Lian,W.T. Zheng and Q. Jiang, *Applied Surface Science* **263** (2012) 260–265.

[10] R. Suryanarayanan, V.M. Naik, P. Kharel, P. Talagala and R. Naik, *Solid State Commun* **133** (2005) 439–443.

[11] F. K. Mohamad Alosfur, M. H. Haji Jumali, S. Radimana, N. J. Ridha and A. Ali Umar, *Procedia Technology* **12** (2014) 264 – 270.